Volume 60
Number 8
25 January 2024
Pages 907–1050

ChemComm

Chemical Communications

rsc.li/chemcomm

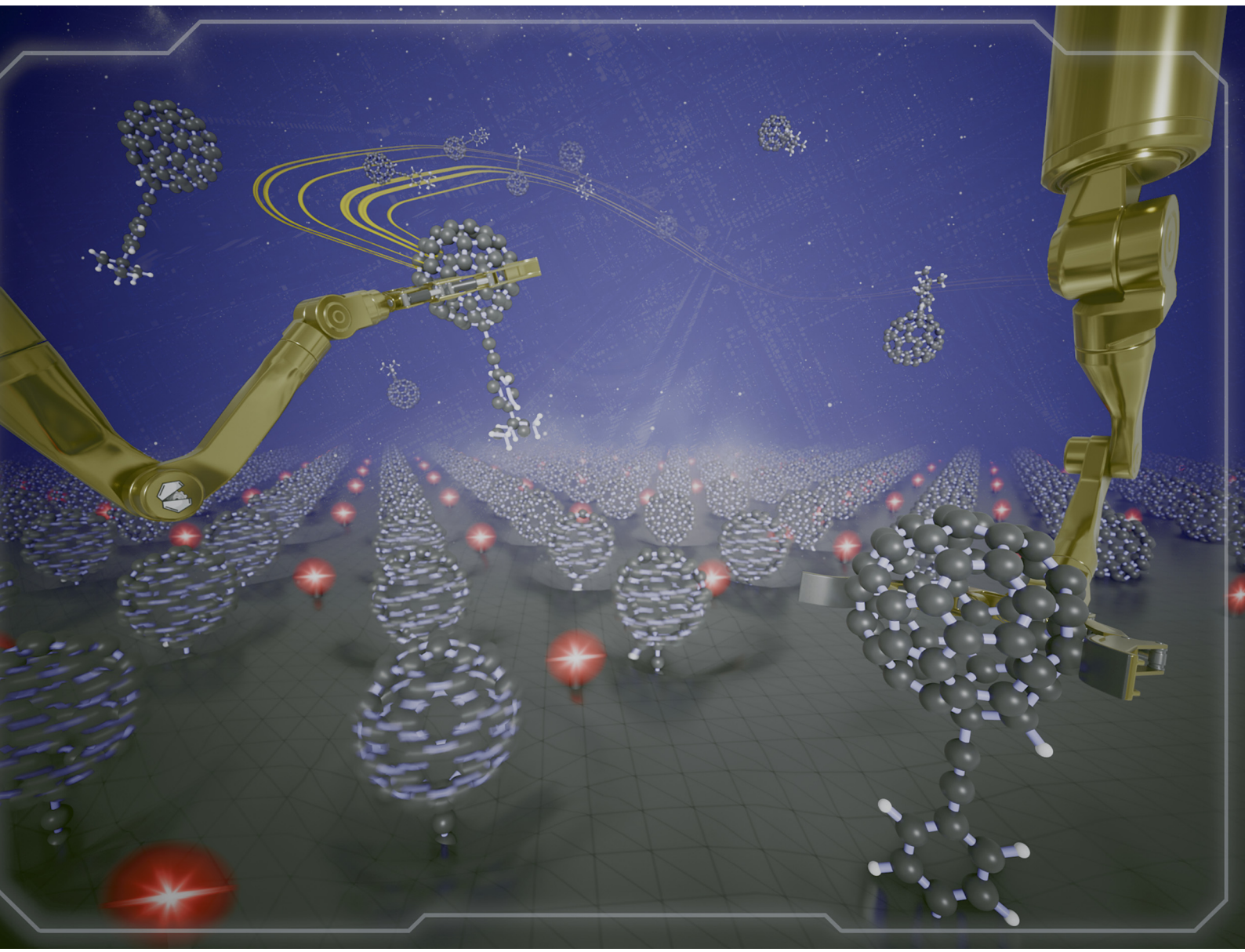

ISSN 1359-7345

ROYAL SOCIETY OF CHEMISTRY

COMMUNICATION

Jiří Kaleta *et al.*

Regular arrays of C_{60}-based molecular rotors mounted on the surface of tris(*o*-phenylenedioxy)cyclotriphosphazene nanocrystals

60 YEARS ANNIVERSARY

ChemComm

COMMUNICATION

View Article Online
View Journal | View Issue

Cite this: *Chem. Commun.*, 2024, **60**, 960

Received 14th September 2023,
Accepted 27th October 2023

DOI: 10.1039/d3cc04559e

rsc.li/chemcomm

Regular arrays of C_{60}-based molecular rotors mounted on the surface of tris(*o*-phenylenedioxy)cyclotriphosphazene nanocrystals†

Carina Santos Hurtado,[a] Guillaume Bastien,[a] Igor Rončević,[b] Martin Dračínský,[a] Teddy Tortorici,[c] Charles T. Rogers,[c] Josef Michl [ad] and Jiří Kaleta *[a]

Dielectric spectroscopy has been used to determine the barriers of rotation of surface-mounted fullerenes (2.3 ± 0.1 and 4.3 ± 0.1 kcal mol^{-1}). In order to achieve this, a C_{60} derivative equipped with an anchoring group designed to form a surface inclusion with the hexagonal form of tris(*o*-phenylenedioxy)cyclotriphosphazene (TPP) has been synthesized. Solid-state NMR analysis revealed that approximately 50% of the surface-mounted molecules have a chemical environment different from the others suggesting two distinct insertion modes. These observations correlate with results of DFT calculations.

Two-dimensional (2-D) regular arrays of functional molecules like rotors, motors and switches represent a unique class of stimuli-responsive materials with exciting properties.[1,2] They attract great attention due to their possible applications in sensing,[3,4] catalysis,[5] molecular machinery,[6,7] molecular electronics,[8,9] *etc.* The construction of such 2-D assemblies is surface-specific and usually requires properly designed molecules.[1,10]

Self-assembly on various (mostly metallic) substrates is probably the most frequently used approach to such arrays on flat surfaces.[11,12] Another widely used technique is based on the preparation of films on water/air interface using a Langmuir–Blodgett trough.[13–16] A third conceptually different approach is based on the installation of molecules on the facets of the hexagonal form of a zeolite-like matrix called tris(*o*-phenylenedioxy)cyclotriphosphazene, often abbreviated as TPP (Chart 1C–E).[17–20] The introduction of sophisticated rod-like molecular anchors allowing the smooth formation of surface inclusions represents another milestone in TPP supramolecular chemistry.[21–23]

In this paper, we are introducing a purely hydrocarbon-based type of "maraca-shaped" rotor molecule **1**, carrying a relatively large dipole moment of ~4.1 D (Chart 1A and B).

The new molecule is comprised of two easily identifiable parts serving distinctly different purposes. (i) Starting from the bottom (Fig. 1A and B), the molecular maraca **1** carries a rigid

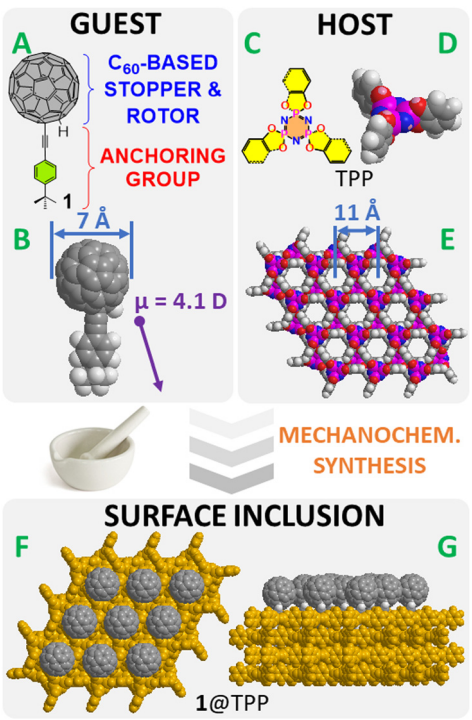

Chart 1 The structure of the C_{60} derivative **1** (A) and its space-filling model with a net dipole moment (B). The structure of the TPP molecule (C), the corresponding space-filling model (D) and a top view of a small fragment of hexagonal TPP (E). An idealized visualization of **1**@TPP: a top (F) and a side (G) view.

[a] *Institute of Organic Chemistry and Biochemistry of the Czech Academy of Sciences, Flemingovo nám. 2, 160 00, Prague 6, Czech Republic. E-mail: jiri.kaleta@uochb.cas.cz*
[b] *Department of Chemistry, University of Oxford, Chemistry Research Laboratory, Oxford OX1 3TA, UK*
[c] *Department of Physics, University of Colorado, Boulder, Colorado 80309, USA*
[d] *Department of Chemistry and Biochemistry, University of Colorado, Boulder, Colorado 80309, USA*

† Electronic supplementary information (ESI) available. See DOI: https://doi.org/10.1039/d3cc04559e

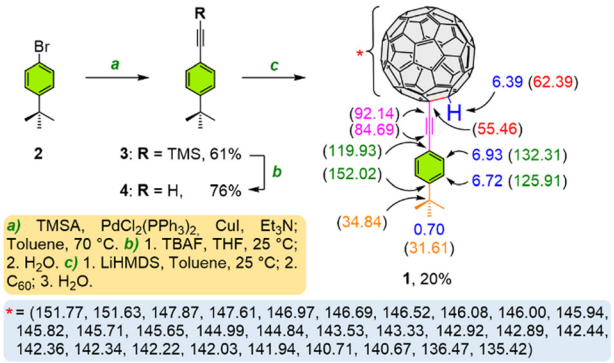

Fig. 1 Synthesis of the C_{60} derivative **1** including complete ^{1}H (blue) and partial ^{13}C NMR (red, purple, green, orange, and black – these colors correspond to the peak labels used in Fig. 3) assignment in **1**.

tail made of 1-(4-*tert*-butyl)-ethynylbenzene acting as an anchoring unit. Its diameter is ~5.0 Å and it nicely fits into the TPP channels, whose internal diameter is ~5.5 Å. The characteristic chemical shifts of the carbon atoms of the *t*-Bu group are also used as nuclear magnetic resonance (NMR) probes during the characterization of supramolecular complexes using solid-state NMR. (ii) The spherical C_{60}-based head with its diameter of ~7 Å is bulky enough to act as a stopper preventing the molecule from complete insertion into the TPP channels. Moreover, it is small enough not to block the neighboring channels and thus to prevent the remaining molecules from entering them (Chart 1E–G). This unit also contributes considerably to the dipole moment, which is calculated to be tilted by ~20° from the axis defined by the two triple-bond carbon atoms (Chart 1B).

Here, we are reporting the synthesis of the molecular rotor **1** and the mechanochemical preparation of surface inclusions differing in surface saturation (50% or 100%). The surface inclusions have been characterized using transmission electron microscopy (TEM), powder X-ray diffraction (PXRD), and solid-state NMR techniques. The ability of individual dipoles to rotate and to respond to an external electric field have been recorded using dielectric spectroscopy. DFT simulations of the surface-mounted **1** in **1**@TPP have shed some light on possible insertion modes and helped rationalize some of the experimental observations.

The synthesis of **1** was a facile process that consisted of Sonogashira cross-coupling between **2** and trimethylsilylacetylene (TMSA), which afforded **3** in a *ca.* 60% yield.[24] The TMS protective group was then removed using TBAF in THF, and the free alkyne **4**[25] was isolated in a nearly 80% yield. The addition of lithium acetylide generated from **4** to a strained C=C bond in C_{60} gave **1** in a relatively high yield (judging based on the ^{1}H NMR of the crude reaction mixture). The yield of isolated **1** was lower due to complications with its separation from the crude reaction mixture (Fig. 1). The structure of the molecular rotor **1** permitted a complete ^{1}H and partial ^{13}C NMR assignment (Fig. 1), which is expected to be useful for examination of future surface inclusions. Not surprisingly, a vast majority of the carbon atoms belonging to the fullerene cannot be unambiguously assigned.

The surface inclusions were prepared using a mechanochemical reaction between crystalline **1** and the hexagonal form of TPP-d_{12}. The mixture of the powdered materials was ball-milled using a planetary ball mill and subsequently annealed under argon atmosphere (see the ESI†).

The morphology of 10%**1**@TPP-d_{12} was determined by TEM. The sample consists of conglomerates of discoidal particles with ~50 nm diameter (Fig. 2A). This is fully consistent with our previous observations.[18,20,21] Based on these results, one facet of a TPP nanocrystal can accommodate up to ~1100 molecular rotors **1**.[21] The 10% molar guest loading represents complete surface saturation.[21] It is well known that the formation of a surface inclusion is usually accompanied by a slight expansion of individual channels in the hexagonal TPP as they adapt to the guest molecules.[20–22,26] These changes can be quantified using the PXRD technique. The PXRD pattern of the 10%**1**@TPP-d_{12} has indeed shown a notable increase of the in-plane spacing parameter *a* (11.598 ± 0.004 Å) and decrease of the layer spacing *c* (9.962 ± 0.006 Å) of the hexagonal TPP (compared to the guest-free material, where *a* = 11.454(5) Å and *c* = 10.160(5) Å),[27] strongly suggesting the formation of a surface inclusion (Fig. 2B). This notable but still relatively small increase further indicates that the molecules of **1** have entered the TPP channels using the *t*-Bu side, ruling out the reverse insertion (the insertion of a fullerene would cause much larger structural changes). The presence of the purely hexagonal TPP phase even after ball milling and annealing also supports the successful formation of inclusion because guest-free hexagonal TPP spontaneously collapses into its more stable monoclinic polymorph. The Lorentzian-shaped diffraction lines observed in Fig. 2B are common for surface inclusions as well.[20,21]

The analytical techniques mentioned so far have revealed the formation of some surface inclusion but do not provide

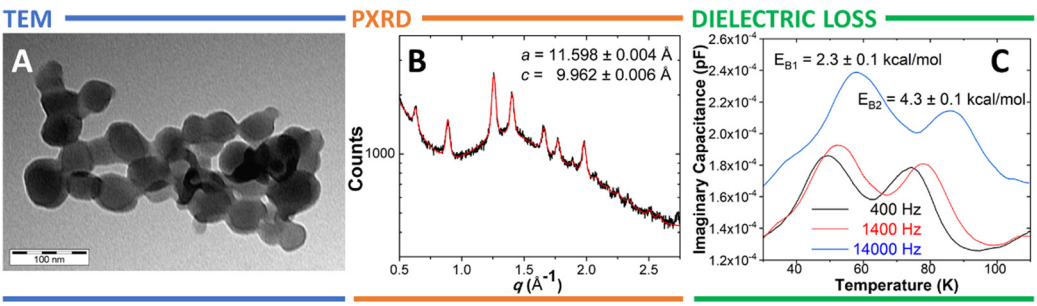

Fig. 2 A TEM visualization of 10%**1**@TPP-d_{12} (A). PXRD pattern of 10%**1**@TPP-d_{12}. The black line represents the diffraction data, while the red curve reflects the fit (B). The dielectric loss of 10%**1**@TPP-d_{12} recorded between 20 and 110 K. Black – 400 Hz, red – 1400 Hz, and blue – 14 000 Hz (C).

information about the depth of insertion and the mutual positions of both components. To answer these questions, solid-state NMR analysis has been performed.

Comparisons of the ^{13}C NMR spectra of the neat guest **1** both in solution and solid state as well as the solid-state spectra of the surface inclusions 5%**1**@TPP-d_{12} and 10%**1**@TPP-d_{12} (Fig. 3) also clearly confirmed formation of expected surface inclusion. Namely, the upfield chemical shifts of carbon atoms from *t*-Bu group that are considered as a characteristic NMR probes and presence of resonances belonging to perdeuteriated TPP matrix in the ^{13}C CP-MAS NMR spectra are particularly indicative. Upfield shifts are characteristic of inclusion complexes because the individual catechol-based aromatic rings forming TPP channels (Chart 1) effectively shield the carbon nuclei of included molecules. Appearance of three resonances representing TPP is due to protiated guest molecules that are in close proximity to the interior of TPP channels and successfully mediate the through-space transfer of polarization from the guest molecules to the carbon atoms of the perdeuteriated matrix. Thorough interpretation of ^{13}C NMR spectra is provided in the ESI.†

The somewhat surprising presence of two inequivalent *t*-Bu groups in both inclusions (Fig. 3C and D) has two possible explanations: (i) all molecules are complexed and approximately half of the guests **1** have a different chemical environment inside the channels from the other half (for example, they are inserted deeper into the TPP matrix)[18] or (ii) half of the molecules form surface inclusion and have a similar chemical environment, while the other half remain uncomplexed. Two additional experiments were performed in order to select one of these hypotheses. Lower molar guest loading in 5%**1**@TPP-d_{12} (5 mol % corresponds to *ca.* 50% statistical occupancy of the portals to the TPP channels) did not affect the ratio of the two species. The same result was achieved once an excess of solvent-free hexagonal TPP-d_{12} was added to 10%**1**@TPP-d_{12} and the sample was ball-milled and annealed again, ruling out the second hypothesis (Fig. S1 and S2, ESI†). Extended annealing of 10%**1**@TPP-d_{12}, which was used to allow the system to equilibrate fully, did not change the ratio of the species either.

To obtain more insight into the behavior of surface-mounted **1** and to rationalize the solid-state NMR results, the structure of **1**@TPP was investigated computationally using a cluster model (details in ESI†). Semiempirical metadynamics followed by reoptimization using the B3LYP functional found three distinct conformers of **1**@TPP, which are shown in Fig. 4A. Complexation energy of these conformers is −50.9 kcal mol^{-1} (**I**), −45.8 kcal mol^{-1} (**II**) and −42.6 kcal mol^{-1} (**III**). To maximize hydrogen bonding, the C_{60} acetylene linker in conformer **I** bends by about 15° relative to the phenylene tail (Fig. 4B).[28] In conformer **II**, only the H···O interaction (d = 2.6 Å) is present, bending is absent and **1** is positioned relatively symmetrically relative to TPP. In **III**, the C_{60} hydrogen points away from TPP, and the rotor **1** again bends to form relatively weak noncovalent interactions with the TPP scaffold.

The anchoring group of **1** in **I** and **II** is immersed much deeper to the TPP matrix than in **III** (6.46 Å for **I** and 6.68 Å for **II** compared to 3.24 Å for **III**), leading to a deshielding of **III** relative to **I** and **II**. DFT averaged calculated chemical shifts of the *t*-Bu carbon atoms (see the ESI†) are 156.92 ppm for structure **I**, 156.47 ppm for structure **II** and 154.84 for structure **III**. This 2 ppm difference in carbon chemical shifts of fully (**I** and **II**) and partially (**III**) inserted **1** is in good agreement with

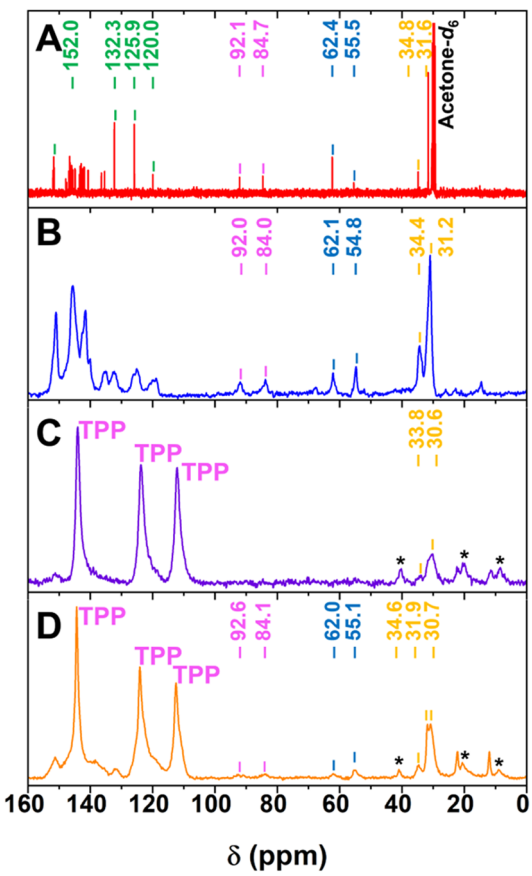

Fig. 3 The ^{13}C NMR spectra of **1** in a CS_2 solution with the internal standard of acetone-d_6 at 25 °C (A), of **1** in solid state (B), and the solid-state ^{13}C CP MAS NMR spectra of 5%**1**@TPP-d_{12} (C) and 10%**1**@TPP-d_{12} (D). The black asterisks indicate spinning sidebands.

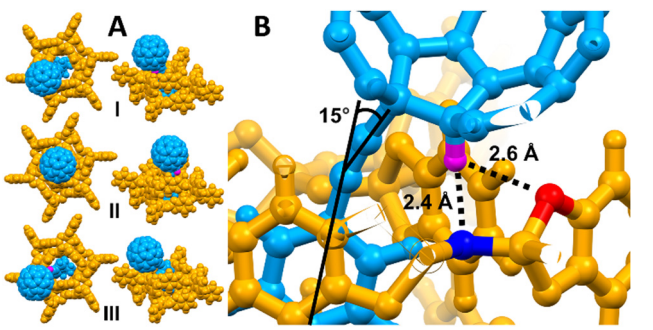

Fig. 4 (A) A side and a top view of the optimized geometries of **1**@TPP conformers obtained at the B3LYP-D3BJ/def2-SVP level of theory. Guest **1** is shown in light blue, TPP in orange, and the hydrogen atom on the C_{60} unit in purple. (B) A detailed view of the bending and hydrogen bonds present in conformer **I** of **1**@TPP.

the experimental finding of two signals separated by 1.2 ppm. On this basis, we hypothesize that the presence of two inequivalent *t*-Bu units in ^{13}C solid-state NMR spectra may be due to different depth of insertion of **1** in TPP. This conclusion cannot be reached by comparing the relative energies of **I–III**, as our calculations do not account for entropy and only locate distinct minima on the potential energy surface.

Rotation requires the cleavage of hydrogen bonds between the C_{60} hydrogen and TPP, resulting in a shared rotational profile for **I** and **II**. Our DFT computations estimate that the barrier associated with this rotation is 5.6 kcal mol^{-1} (Fig. S3a, ESI†). Configuration **III** is predicted to rotate almost freely (E_{rot} = 0.4 kcal mol^{-1}; Fig. S3b, ESI†), and it can interconvert to **I** by translation through the channel, which has a calculated barrier of 8.7 kcal mol^{-1} (Fig. S4, ESI†).

Individual molecular guests **1** carry relatively large permanent dipoles (~4.1 D calculated using DFT – see Table S1, ESI†). Therefore, their response to an external electric field (particularly once arranged in a 2-D array in 10%**1**@TPP-d_{12}) can be monitored using dielectric spectroscopy. The unique geometry of such 2-D assemblies usually guarantees individual molecules (located on the solid–gas interface) sufficient separation from neighbors and thus relatively unrestricted rotation. The rotational barriers were extracted from the positions of the associated dielectric-loss peaks for different external-field frequencies. The dielectric loss of 10%**1**@TPP-d_{12} has shown two distinct peaks between *ca.* 30 and 100 K (Fig. 2C), with the first one slightly more populated than the one at higher temperature. They are associated with two rather low barriers of rotation: 2.3 ± 0.1 (E_{B1}) and 4.3 ± 0.1 kcal mol^{-1} (E_{B2}). These barriers likely correspond to the rotation of the weakly bound conformer **III** (E_{B1}) and the more deeply inserted complexes **I** and **II** (E_{B2}). The computed barriers (Fig. S3, ESI†) for these processes ($E_{rot,III}$ = 0.4 kcal mol^{-1}; $E_{rot,I}$ = 5.6 kcal mol^{-1}) are in reasonable agreement with measured values of E_{B1} and E_{B2} (2.3 and 4.3 kcal mol^{-1}), given the accuracy of empirically-corrected DFT and the neglect of entropy.

To conclude, we have synthesized a unique type of fullerene-based molecular rotor **1** with a relatively high dipole moment. This compound was successfully inserted into the hexagonal TPP matrix, resulting in **1**@TPP-d_{12} surface inclusions, where the rod-like section of the molecule acted as an anchor and the fullerene unit stayed above the surface. It has been found that approximately half of the molecules of **1** have a chemical environment different from the other half. The DFT simulations of **1**@TPP-d_{12} indicate that part of the guest molecules is immersed relatively deeply, their molecular axis is parallel with the axis of the TPP channel and only the fullerene part is slightly tilted because of the hydrogen bonds between the C_{60}-H and the heteroatoms present in the TPP matrix. The other guest molecules are inserted only shallowly, and their molecular axis is noticeably tilted. The two experimentally determined rotation barriers (*ca.* 2 and 4 kcal mol^{-1}) most likely correspond to the rotation of C_{60}-based dipoles in complexes with different TPP penetration depth.

This work was supported by the Institute of Organic Chemistry and Biochemistry of the Czech Academy of Sciences (RVO: 61388963), the Czech Science Foundation (grant number: 20-13745S), and the Ministry of Education, Youth and Sports (grant number: LTAUSA19120). Computational resources were provided by the Ministry of Education, Youth and Sports of the Czech Republic through the e-INFRA CZ (ID:90254). We thank Prof. Gang Cao and Mr Yu Zhang for access to the Rigaku Miniflex 600 system and for helpful conversations about the powder X-ray patterns presented in this study. We are thankful to Dr Lukáš Severa for calculating the dipole moments of the guest.

Conflicts of interest

There are no conflicts to declare.

References

1 J. Kaleta, Molecular Switches and Motors in 2-D, in *Molecular Photoswitches*, ed. Z. L. Pianowski, Wiley-VCH GmbH, 2022.
2 R. Klajn, *Pure Appl. Chem.*, 2010, **82**, 2247–2279.
3 R. Arumugaperumal, W. L. Hua, P. Raghunath, M. C. Lin and W. S. Chung, *ACS Appl. Mater. Interfaces*, 2020, **12**, 29650–29660.
4 M. Martínez-Abadía, R. Giménez and M. B. Ros, *Adv. Mater.*, 2018, **30**, 1704161.
5 K. Grill and H. Dube, *J. Am. Chem. Soc.*, 2020, **142**, 19300–19307.
6 S. Corra, M. Curcio, M. Baroncini, S. Silvi and A. Credi, *Adv. Mater.*, 2020, **32**, 1906064.
7 V. García-López, D. Liu and J. M. Tour, *Chem. Rev.*, 2020, **120**, 79–124.
8 D. Xiang, X. Wang, C. Jia, T. Lee and X. Guo, *Chem. Rev.*, 2016, **116**, 4318–4440.
9 Z. Chai, A. Childress and A. A. Busnaina, *ACS Nano*, 2022, **16**, 17641–17686.
10 T. R. Rusch, M. Hammerich, R. Herges and O. M. Magnussen, *Chem. Commun.*, 2019, **55**, 9511–9514.
11 J. A. A. W. Elemans, S. Lei and S. De Feyter, *Angew. Chem., Int. Ed.*, 2009, **48**, 7298–7332.
12 C. J. Love, L. A. Estroff, J. K. Kriebel, R. G. Nuzzo and G. M. Whitesides, *Chem. Rev.*, 2005, **105**, 1103–1170.
13 J. Mao, O. Ortiz, J. Wang, A. Malinge, A. Badia and S. Kéna-Cohen, *Nanoscale*, 2020, **12**, 19814–19823.
14 E. Kaletová, C. Santos Hurtado, I. Císařová, S. J. Teat and J. Kaleta, *ChemPlusChem*, 2022, **87**, e202200023.
15 J. Kaleta, J. Wen, T. F. Magnera, P. I. Dron, C. Zhu and J. Michl, *Proc. Natl. Acad. Sci. U. S. A.*, 2018, **115**, 9373–9378.
16 O. N. Oliveira, L. Caseli and K. Ariga, *Chem. Rev.*, 2022, **112**, 6459–6513.
17 S. Bracco, A. Comotti, L. Ferreti and P. Sozzani, *J. Am. Chem. Soc.*, 2011, **133**, 8982–8994.
18 P. Sozzani, S. Bracco, A. Comotti, L. Ferretti and R. Simonutti, *Angew. Chem., Int. Ed.*, 2005, **44**, 1816–1820.
19 L. Kobr, K. Zhao, Y. Shen, A. Comotti, S. Bracco, R. K. Shoemaker, P. Sozzani, N. A. Clark, J. C. Price, C. T. Rogers and J. Michl, *J. Am. Chem. Soc.*, 2012, **134**, 10122–10131.
20 J. Kaleta, G. Bastien, J. Wen, M. Dračínský, E. Tortorici, I. Císařová, P. D. Beale, C. T. Rogers and J. Michl, *J. Org. Chem.*, 2019, **84**, 8449–8467.
21 J. Kaleta, J. Chen, G. Bastien, M. Dračínský, M. Mašát, C. T. Rogers, B. L. Feringa and J. Michl, *J. Am. Chem. Soc.*, 2017, **139**, 10486–10498.
22 C. Santos Hurtado, G. Bastien, M. Mašát, J. R. Štoček, M. Dračínský, I. Rončević, I. Císařová, C. T. Rogers and J. Kaleta, *J. Am. Chem. Soc.*, 2020, **142**, 9337–9351.
23 J. Kaleta, P. I. Dron, K. Zhao, Y. Shen, I. Císařová, C. T. Rogers and J. Michl, *J. Org. Chem.*, 2015, **80**, 6173–6192.
24 A. H. Sato, S. Mihara and T. Iwasawa, *Tetrahedron Lett.*, 2012, **53**, 3585–3589.
25 N. O. Thiel, S. Kemper and J. F. Teichert, *Tetrahedron*, 2017, **73**, 5023–5028.
26 K. Zhao, P. I. Dron, J. Kaleta, C. T. Rogers and J. Michl, *Top. Curr. Chem.*, 2014, **354**, 163–212.
27 A. Comotti, S. Bracco, L. Ferretti, M. Mauri, R. Simonutti and P. Sozzani, *Chem. Commun.*, 2007, 350–352.
28 I. Rončević, E. Kaletová, K. Varga, I. Císařová, Z. Bastl, J.-C. Jiang and J. Kaleta, *J. Phys. Chem. C*, 2022, **126**, 7193–7207.